

Current Induced Switching of Superconducting Order and Enhancement of Superconducting Diode Efficiency

Uddalok Nag,¹ Jonathan Schirmer,² Chao-Xing Liu,^{1,3} and J. K. Jain^{1,3}

¹*Department of Physics, 104 Davey Lab, The Pennsylvania State University, University Park, Pennsylvania 16802, USA*

²*Department of Physics, William & Mary, Williamsburg, Virginia 23187, USA*

³*Center for Theory of Emergent Quantum Matter, The Pennsylvania State University, University Park, Pennsylvania 16802, USA*

We propose that the superconducting diode (SD) efficiency can be significantly enhanced near the transition between two superconducting states by choosing parameters where, before the system goes normal with increasing supercurrent, it switches into a different superconducting order for one direction of the current but not for the other. This mechanism for producing high SD efficiency relies on the expectation that the critical current depends sensitively on the superconducting order. We demonstrate this explicitly by performing detailed calculations for a bilayer superconductor with an in-plane magnetic field, which admits the standard Bardeen-Cooper-Schrieffer (BCS) and the orbital Fulde-Ferrell-Larkin-Ovchinnikov (FFLO) orders as a function of the strength of the magnetic field. We predict a sharp peak in the SD efficiency in the FFLO state close to the transition, which arises from a complex interplay between the two superconducting orders. An implication of our study is that the measurement of the SD efficiency can provide fundamental insight into the nature of the BCS-FFLO transition both as a function of the magnetic field and the supercurrent.

Introduction - In the superconducting (SC) state, the condensation of Cooper pairs allows electric current to flow without energy dissipation, thereby producing a “zero resistance” state that is a defining feature of superconductivity [1]. This supercurrent is the basis for a variety of potential applications of superconductors, including lossless power transmission [2], high-field SC magnets [3], quantum devices such as SQUIDs and SC qubits [4], and precision sensors for scientific and medical technologies [5]. A superconductor undergoes a transition to the normal state when the supercurrent exceeds a critical value, a phenomenon often attributed to pair-breaking effects [1, 6, 7]. In conventional superconductors, the critical depairing current is typically reciprocal, that is, its magnitude remains the same for currents flowing in opposite directions. Recent theory and experiments [8–20] have discovered nonreciprocity of dissipationless supercurrent in certain SC materials, where the supercurrent flows in one direction but not the opposite, a phenomenon called “superconducting diode effect” in analogy to the nonreciprocal transport in a semiconducting diode. The superconducting diode (SD) efficiency is defined as

$$\eta = |I_c^+ - I_c^-| / (I_c^+ + I_c^-), \quad (1)$$

where I_c^\pm are the critical currents in two opposite directions. Similarly to the central role of semiconducting diodes in modern electronic technologies, the SD effect may have potential device applications in superconducting rectifiers [21] and logic circuits [22], cryogenic computing, and low-loss energy conversion systems [9, 23].

The objective of the present work is to propose a mechanism to enhance the SD efficiency near the transition between two distinct SC states, denoted as SC_1 and SC_2 , in the parameter regime when a SC_1 -normal

transition occurs as the current increases in one direction, but a SC_1 - SC_2 -normal transition occurs in the opposite direction. The enhancement of SD efficiency occurs because of the critical current depends sensitively on the superconducting order. As an explicit demonstration, we consider a bilayer superconductor with an in-plane magnetic field, which has been shown to admit two types of SC orders. At low magnetic fields the phases of the order parameters in two layers are equal, which we refer to as the Bardeen-Cooper-Schrieffer (BCS) state. As the magnetic field is increased, its coupling to the electron motion induces a transition into an *orbital* Fulde-Ferrell-Larkin-Ovchinnikov (FFLO) state with finite momentum pairing, as was predicted by Ref. [24], where a spatially varying phase difference exists between two layers [24]. Evidence for this state has been revealed by probing rotational symmetry breaking in the SC state [25, 26]. Further theoretical work has revealed the important role of interlayer vortices in the transition regime from the BCS state to the orbital FFLO state [27]. (We neglect throughout this paper the Zeeman coupling of magnetic field to the electron spin, as is valid for the class of non-centrosymmetric layered superconductors known as Ising superconductors; here, strong Ising SOC pins electron spin into the out-of-plane direction and thus suppresses the Zeeman effect of in-plane magnetic fields, leading to a high upper critical field several times above the Pauli limit [25, 28–30].)

It is well known that increasing the supercurrent through a superconductor drives a transition into the normal state beyond a critical current. We show below that, for magnetic fields when two types of superconducting orders are in close competition, it is possible that increasing the supercurrent in one direction switches FFLO into BCS before the system eventually becomes normal, but

in the opposite direction, the transition happens from FFLO to normal directly. We find a marked enhancement of the SD efficiency in this regime.

We emphasize that the enhancement mechanism of SD effect considered here differs from that associated with the FFLO state discussed in Ref. [14–16, 20, 31]. These consider a class of non-centrosymmetric superconductors, where the interplay between the Rashba spin-orbit coupling (which produces spin-textured Fermi surfaces) and the Zeeman splitting from in-plane magnetic fields can drive a spatial modulation of the *overall* SC phase, yielding the so-called helical SC state or single- \mathbf{q} FFLO state [14, 32–34]. The momentum \mathbf{q} in the FFLO imposes a directional asymmetry in the critical current, which naturally results in SD effect [14]. In contrast, the *orbital* FFLO state in a SC bilayer considered here involves a *relative* phase shift of SC order parameters between the two layers rather than an overall phase modulation, and hence does not by itself produce an SD

effect. In our case, the enhancement of SD effect near the BCS–FFLO transition arises from the coupling between interlayer vortices and the net supercurrent when inversion symmetry between two layers is broken.

Phase diagram as a function of current and magnetic field – We now describe how we obtain the phase diagram of a SC bilayer in the presence of a supercurrent and an in-plane magnetic field by solving the Ginzburg–Landau (GL) equations self-consistently. We denote the SC order parameters in the layer $l = 1, 2$ as $\Psi_l = \psi_l e^{i(\xi(x) - (-1)^l \phi(x)/2 + qx)}$, where the amplitude ψ_l is taken to be spatially uniform (previous calculations have shown a very weak dependence on x in the FFLO state [27]), $\xi(x)$ and $\phi(x)$ are periodic over the length L_x of the system and describe the overall and relative phases between two layers. We also add the phase e^{iqx} to control the current through the system. Based on the order parameter form, the Ginzburg–Landau (GL) free energy is written as

$$\Omega[\Psi_l] = \frac{1}{V_0} \int d^2\mathbf{r} \left[\sum_l \alpha_l \psi_l^2 + \frac{\beta}{2} \sum_l \psi_l^4 + \frac{\psi_1^2}{2m} \left(q - q_B + \frac{\nabla\phi}{2} \right)^2 + \frac{\psi_2^2}{2m} \left(q + q_B - \frac{\nabla\phi}{2} \right)^2 - 2J\psi_1\psi_2 \cos\phi \right], \quad (2)$$

where α_l controls the onset of superconductivity in layer l and changes sign at the mean field transition temperature ($\alpha_l \propto (T - T_{c,l})$), the fourth order term $\beta > 0$ to ensure that the system is stable, m is the cooper pair mass and J is the strength of the interlayer Josephson coupling. We allow $\alpha_1 \neq \alpha_2$ to break the inversion symmetry between two layers. To describe an in-plane magnetic field $\mathbf{B} = B\hat{e}_y$, we also include the vector potential $\mathbf{A}_l = (-1)^l \frac{d}{2} \mathbf{B} \times \hat{e}_z = (-1)^l \frac{dB}{2} \hat{e}_x$, where d is the separation between the two layers, and introduce the parameter $q_B = edB = 2\pi\Phi/(L_x\Phi_0)$, where Φ is the net flux between two layers in the system of length L_x and $\Phi_0 = hc/e$ is the flux quantum. For a given q_B , the density of magnetic flux quanta is given by $\Phi/(L_x\Phi_0) = q_B/(2\pi)$. We consider periodic boundary conditions in the x direction. The periodic overall phase $\xi(x)$ can be gauged away by making the replacement $A_l \rightarrow A'_l = A_l - \frac{1}{2e}\nabla\xi(x)$ for both layers.

We need to minimize the GL free energy with respect to ψ_1 , ψ_2 and $\phi(x)$ for fixed q and q_B , and we refer to the minimum energy as the condensation energy $E_{\text{con}}(q, q_B)$. Variation with respect to $\phi(x)$ produces the sine-Gordon (SG) equation

$$\partial_w^2 \phi = \sin\phi \quad (3)$$

where $w = (4J'm')^{1/2}x$ is a rescaled length, with $m' = 2m/(\psi_1^2 + \psi_2^2)$ and $J' = \psi_1\psi_2J$. As discussed in Sec. (S2) of Supplementary Material (SM) [35], the solutions

of the SG equation are given by

$$\phi = 2 \text{am} \left(\pm \frac{1}{k} w, k^2 \right) - \pi, \quad (4)$$

where am is the Jacobi amplitude function [36, 37]. The parameter $0 < k \leq 1$ controls the density of vortices per unit length, $\rho = \sqrt{J'm'}/(kK(k^2))$, where K is the complete elliptic integral of the first kind [36, 37] and a single vortex refers to a rotation of ϕ by 2π . The trivial phase-locked solution $\phi = 0$ ($\rho = 0$) is obtained for $k = 1$, as $K(k^2)$ diverges logarithmically as $k \rightarrow 1$; this will be referred to as the BCS state. The state in which ϕ varies with x contains interlayer vortices and corresponds to the (orbital) FFLO state [24, 25].

We next substitute Eq. (4) into the expression for the GL free energy Ω in Eq.(2) and minimize it with respect to ψ_1 , ψ_2 and k (k fixes ϕ) numerically for given q and q_B to get $E_{\text{con}}(q, q_B)$, shown in the upper panels of Fig. 1 for different values of q_B . The supercurrent is given by $I_x = 2e(\partial\Omega/\partial q)_{\text{min}} = 2e\partial E_{\text{con}}/\partial q$,

$$I_x = \frac{2e}{m} [(\psi_1^2 + \psi_2^2)q - (\psi_1^2 - \psi_2^2)(q_B - \nabla\phi/2)]_{\text{min}}, \quad (5)$$

where the subscript min implies evaluation at values of ψ_l and ϕ that minimize the free energy. [In all the figures shown, we normalize the value of the current by the critical current at zero magnetic field, $I_c^+(0)$; at $q_B = 0$, the critical current is same in both directions due to time-reversal symmetry]. The supercurrent is shown in the

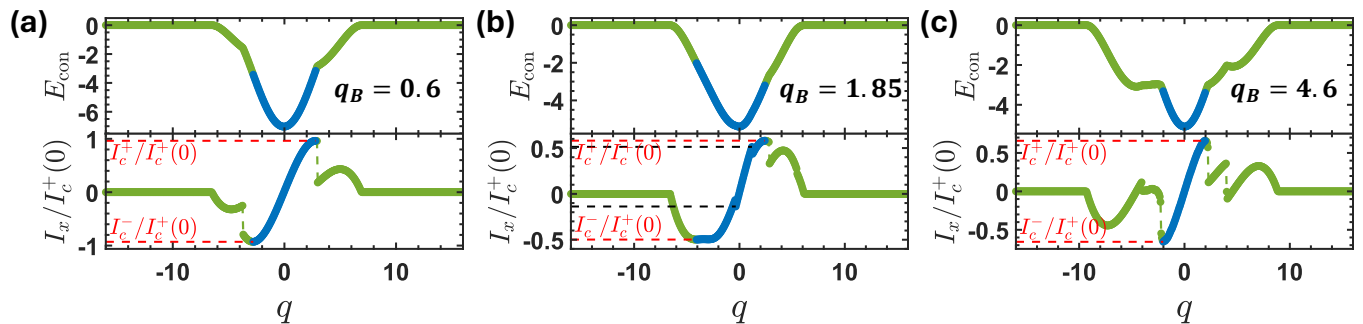


FIG. 1: *Upper panels:* Ground state energy E_{con} versus momentum q . The results are shown for a bilayer with asymmetry parameter $a = 0.1$ at three magnetic field (q_B) values. *Lower panels:* Supercurrent $I_x = 2e\partial E_{\text{con}}/\partial q$ versus q . When a given I_x is produced by more than one value of q , we choose q corresponding to the lowest energy, highlighted in blue. Critical currents I_c^+ and I_c^- (marked in red) correspond to the maximum supercurrent. Black dashed lines mark phase boundaries between FFLO and BCS orders. (a) $q_B = 0.6$: The system remains in the BCS state for all current values. (b) $q_B = 1.85$: At zero current, the system is in the FFLO state. Increasing current in either direction induces a transition into the BCS state (crossing the black dashed lines) before ultimately driving the system normal. (c) $q_B = 4.2$: The system remains in the FFLO state for all current values.

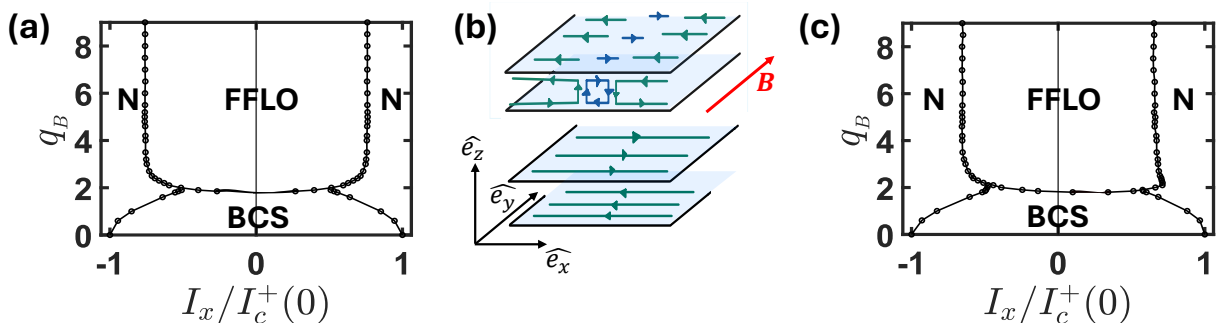


FIG. 2: (a) Phase diagram of the symmetric bilayer ($\alpha_1 = \alpha_2 = -10$) as a function of the current I_x (in units of $I_c^+(0)$, the critical current at zero magnetic field) and $q_B \propto B$ (q_B is 2π times the number of magnetic flux quanta per unit length). The BCS and FFLO states separated by second-order transitions, and by first-order transitions from the normal (N) state at high currents. (b) Schematic illustration of the BCS state with uniform interlayer phase ($\phi = 0, \rho = 0$, bottom) and FFLO state with spatially varying interlayer phase ($\phi \neq 0, \rho \neq 0$, top). Green/blue arrows indicate local current patterns at $I_x = 0$. The in-plane magnetic field is $\mathbf{B} = B\hat{e}_y$. (c) Phase diagram of an asymmetric bilayer ($\alpha_1 = -9, \alpha_2 = -11$), which does not have inversion symmetry. The phase boundaries are asymmetric about $I_x = 0$, yielding unequal critical currents I_c^+ and I_c^- and thus a nonzero superconducting diode efficiency. For both phase diagrams: $\beta = 20, J = 2, m = 1$ (these parameters are defined in main text and related to microscopic quantities in in Sec. (S1) of the SM)

lower panels of Fig. 1. In cases when multiple values of q yield the same current, we select the q (highlighted in blue) with the lowest energy. The critical currents I_c^+ and I_c^- can be read off directly from Fig. 1.

We display the phase diagram in the q_B - I_x plane in Fig. 2. Panel (a) shows the phase diagram for a symmetric bilayer ($\alpha_1 = \alpha_2$), while panel (c) for an asymmetric bilayer with the asymmetry factor $a = |(\alpha_1 - \alpha_2)/(\alpha_1 + \alpha_2)| = 0.1$. At small B , the system is in the BCS state with no interlayer vortices ($\phi = 0$), but it makes a transition with increasing B into the FFLO state with interlayer vortices.

At fixed B (fixed q_B), as the current I_x exceeds a crit-

ical value, there is a transition into the normal state. Interestingly, however, for certain values of q_B , the system can switch from FFLO to BCS as the current is increased, before being driven normal. Even re-entrant transitions like BCS-FFLO-BCS-normal are possible [see the inset of Fig. 3(a) which is zoomed-in region of Fig. 2(c)]. Such current induced switching of the superconducting order lies at the root of the enhancement of SD efficiency, as discussed below.

Superconducting diode efficiency - The SD efficiency η , defined in Eq. (1), is zero whenever the second term inside the square brackets in Eq.(5), which describes the Meissner current, is zero. That, in turn, is the case when

(i) the system has inversion symmetry ($\psi_1 = \psi_2$); or (ii) $q_B = 0$; or (iii) the Abrikosov vortex density is $\rho = 2q_B/(2\pi)$, i.e. equal to twice the number of magnetic flux quanta passing through the layers. In general, the evaluation of η requires a detailed calculation. Fig. 3 shows the SD efficiency η as a function of the magnetic field for several values of the asymmetry parameter a .

For small q_B , the system is in the BCS state with $\phi = 0$ and we note a linear increase of η as a function of q_B . This follows from Eq. (5) with $\phi = 0$, provided that ψ_1 and ψ_2 are independent of q_B to leading order, which is shown to be the case in Sec. (S3) of the SM.

As a reference, let us take the model considered in Ref. [24] which studied the BCS-FFLO transition by assuming that the vortex density in the FFLO state is given by twice the magnetic flux density. In this model, η increases with q_B in the BCS state, but drops discontinuously to zero as soon as the system makes a transition into the FFLO state.

Our results for η are qualitatively different. Remarkably, for small a , η actually increases rapidly, rather than dropping to zero, as the system enters the FFLO state, but at some point it begins to decrease rapidly, approaching zero at large q_B . The most striking feature is a sharp peak in η on the FFLO side of the transition. In a broad sense, this physics arises only with the more detailed treatment of the BCS-FFLO transition in terms of the sine-Gordon model, wherein the vortex density rises continuously from zero to twice the magnetic flux density [see Fig. 3 (b) and its inset and Sec. (S6) of SM]. Furthermore, the enhancement can be seen to occur in the region where the superconducting order switches from FFLO to BCS as the supercurrent is increased in one direction while remains in the FFLO in the other. In the insets of Fig. 3(a), this region is marked between two horizontal dashed lines, blue (green) for $a = 0.1$ ($a = 0.2$), which correspond to the vertical dashed lines in the main figure. We attribute the enhanced SD efficiency to the sensitive dependence of the supercurrent to the type of superconducting order, which enhances the asymmetry in this region.

It is intuitively expected that there are two vortices per magnetic flux quantum in the limit $q_B \rightarrow \infty$, implying that η vanishes here. Mathematically, the limit $q_B \rightarrow \infty$ can be shown to be equivalent to $J \rightarrow 0$ (see Sec. (S5) of SM), where the two layers effectively decouple. For $J = 0$, minimization with respect to ϕ yields $\nabla\phi(x) \rightarrow 2q_B x$, which corresponds to the vortex density $\rho = 2q_B/(2\pi)$, which is equal to twice the number of magnetic flux quanta passing through the layers. With this form of ϕ , and with $J = 0$, Ω is an even function of q , i.e. the current is an odd function of q , implying $\eta = 0$. For details, see Sec. (S4) of the SM where we prove up to the order of $1/q_B^3$.

Conclusion and Discussion - In summary, we have demonstrated that a supercurrent can induce a BCS-

FFLO transition in a SC bilayer under in-plane magnetic fields. This current-induced transition is asymmetric with respect to two current directions, leading to an enhancement of SD efficiency.

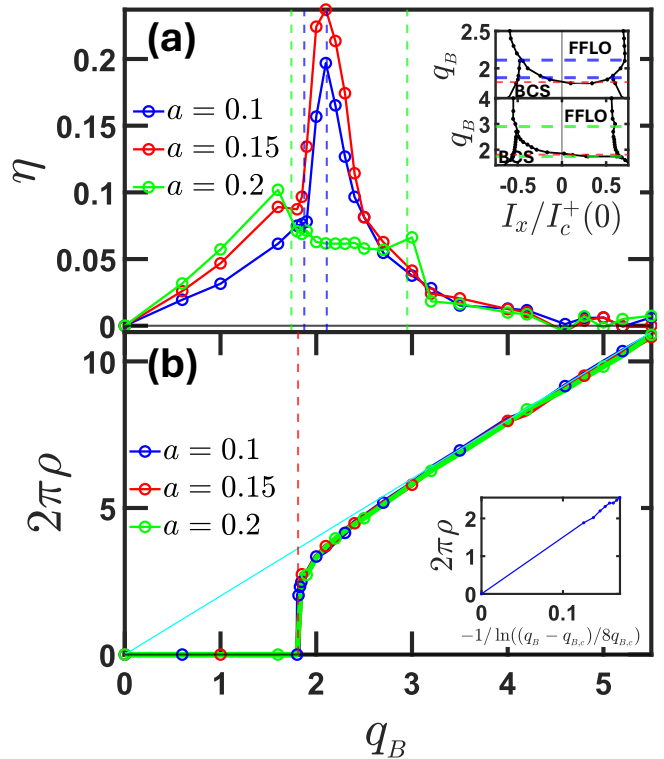


FIG. 3: (a) Superconducting diode efficiency η as a function of magnetic field q_B for various values of asymmetry parameter $a = |(\alpha_1 - \alpha_2)/(\alpha_1 + \alpha_2)|$. The upper (lower) inset shows magnified phase diagram from Fig. 2(c) at $a = 0.1$ ($a = 0.2$). In both insets, the region between the horizontal dashed lines (blue for $a = 0.1$, green for $a = 0.2$) marks the q_B range where current in the $+x$ direction induces a FFLO \rightarrow N transition while current in the $-x$ direction induces a FFLO \rightarrow BCS \rightarrow N transition. These lines correspond to the color-matched vertical dashed lines in the main panel, marking the region of enhanced η . (b) Interlayer vortex density ρ as a function of magnetic field q_B at $I_x = 0$. The light blue line shows the high-field limiting case $\rho = 2q_B$, corresponding to maximum vortex density where the layers effectively decouple. The vertical red dashed line marks the value of q_B at which vortices start entering the system at zero current. The inset depicts the vortex density ρ plotted as a function of $-1/\ln[(q_B - q_{B,c})/8q_{B,c}]$, in accordance with the asymptotic behavior derived in Eq. (S84) in Sec. (S6) of the SM for $a = 0.1$, to make it evident that the vortices enter the system continuously.

Our mechanism relies on interlayer vortices generated by the orbital effect of in-plane magnetic field in combi-

nation with interlayer Josephson coupling, and thus does not, in principle, require spin-orbit coupling. It is distinct from the existing theories of SD effect relying on strong spin-orbit coupling and Zeeman effects [14, 20] and thus broadens the range of systems in which an enhanced SD efficiency may be realized. Our prediction are directly relevant to recent experiments on layered superconductors with orbital FFLO state [13, 25, 26, 38, 39].

An important implication of our work is that the measurement of the SD efficiency provides fundamental insight, and can thus serve as a probe into the nature of the phase transition. As noted above, a sharp peak in η on the FFLO side is an indication of the continuous nature of the BCS-FFLO transition, as well as of a supercurrent induced FFLO-BCS transition. Finally, we expect similar enhancement of the SD efficiency in other systems with competing superconducting orders, but leave detailed studies for future work.

Acknowledgments - We gratefully acknowledge Dr. Debmalaya Chakraborty for insightful discussions. UN and JKJ were supported in part by the U. S. Department of Energy, Office of Basic Energy Sciences, under Grant no. DE-SC0005042. JS was supported by the U.S. US Department of Energy, Office of Basic Energy Sciences, via Award No. DE-SC0022245. C.-X.L acknowledges the support from the NSF through The Pennsylvania State University Materials Research Science and Engineering Center [DMR-2011839]. We acknowledge Advanced CyberInfrastructure computational resources provided by The Institute for CyberScience at The Pennsylvania State University.

-
- [1] M. Tinkham. *Introduction to Superconductivity*. McGraw-Hill, 2 edition, 1996.
- [2] RW Meyerhoff. Superconducting power transmission. In *The Science and Technology of Superconductivity: Proceedings of a summer course held August 13–26, 1971, at Georgetown University, Washington, DC*, pages 433–458. Springer, 1973.
- [3] Fred M Ašner. *High field superconducting magnets*. Oxford University Press, 1999.
- [4] Chui-Ping Yang, Shih-I Chu, and Siyuan Han. Possible realization of entanglement, logical gates, and quantum-information transfer with superconducting-quantum-interference-device qubits in cavity qed. *Physical Review A*, 67(4):042311, 2003.
- [5] Sergey Danilin, Nicholas Nugent, and Martin Weides. Quantum sensing with tunable superconducting qubits: optimization and speed-up. *New Journal of Physics*, 26(10):103029, 2024.
- [6] Philip F. Bagwell. Critical current of a one-dimensional superconductor. *Physical Review B*, 49:6841–6846, 3 1994. ISSN 0163-1829. doi:10.1103/PhysRevB.49.6841.
- [7] A. Gurevich. Limits of the upper critical field in dirty two-gap superconductors. *Physica C: Superconductivity*, 456:160–169, 6 2007. ISSN 09214534. doi:10.1016/j.physc.2007.01.008.
- [8] Yuan Cao, Valla Fatemi, Shiang Fang, Kenji Watanabe, Takashi Taniguchi, Efthimios Kaxiras, and Pablo Jarillo-Herrero. Unconventional superconductivity in magic-angle graphene superlattices. *Nature*, 556:43–50, 4 2018. ISSN 0028-0836. doi:10.1038/nature26160.
- [9] Fuyuki Ando, Yuta Miyasaka, Tian Li, Jun Ishizuka, Tomonori Arakawa, Yoichi Shiota, Takahiro Moriyama, Youichi Yanase, and Teruo Ono. Observation of superconducting diode effect. *Nature*, 584:373–376, 8 2020. ISSN 0028-0836. doi:10.1038/s41586-020-2590-4.
- [10] Margarita Davydova, Saranesh Prembabu, and Liang Fu. Universal josephson diode effect. *Science Advances*, 8, 6 2022. ISSN 2375-2548. doi:10.1126/sciadv.abo0309.
- [11] Akito Daido, Yuhei Ikeda, and Youichi Yanase. Intrinsic superconducting diode effect. *Physical Review Letters*, 128:037001, 1 2022. ISSN 0031-9007. doi:10.1103/PhysRevLett.128.037001.
- [12] James Jun He, Yukio Tanaka, and Naoto Nagaosa. A phenomenological theory of superconductor diodes. *New Journal of Physics*, 24:053014, 5 2022. ISSN 1367-2630. doi:10.1088/1367-2630/ac6766.
- [13] Lorenz Bauriedl, Christian Bäuml, Lorenz Fuchs, Christian Baumgartner, Nicolas Paulik, Jonas M. Bauer, Kai-Qiang Lin, John M. Lupton, Takashi Taniguchi, Kenji Watanabe, Christoph Strunk, and Nicola Paradiso. Supercurrent diode effect and magnetochiral anisotropy in few-layer nbse2. *Nature Communications*, 13:4266, 7 2022. ISSN 2041-1723. doi:10.1038/s41467-022-31954-5.
- [14] Noah F. Q. Yuan and Liang Fu. Supercurrent diode effect and finite-momentum superconductors. *Proceedings of the National Academy of Sciences*, 119, 4 2022. ISSN 0027-8424. doi:10.1073/pnas.2119548119.
- [15] Banabir Pal, Anirban Chakraborty, Pranava K. Sivakumar, Margarita Davydova, Ajesh K. Gopi, Avanindra K. Pandeya, Jonas A. Krieger, Yang Zhang, Mihir Date, Sailong Ju, Noah Yuan, Niels B. M. Schröter, Liang Fu, and Stuart S. P. Parkin. Josephson diode effect from cooper pair momentum in a topological semimetal. *Nature Physics*, 18:1228–1233, 10 2022. ISSN 1745-2473. doi:10.1038/s41567-022-01699-5.
- [16] Yasen Hou, Fabrizio Nichele, Hang Chi, Alessandro Lodesani, Yingying Wu, Markus F. Ritter, Daniel Z. Haxell, Margarita Davydova, Stefan Ilić, Ourania Glezakou-Elbert, Amith Varambally, F. Sebastian Bergeret, Akashdeep Kamra, Liang Fu, Patrick A. Lee, and Jagadeesh S. Moodera. Ubiquitous superconducting diode effect in superconductor thin films. *Physical Review Letters*, 131:027001, 7 2023. ISSN 0031-9007. doi:10.1103/PhysRevLett.131.027001.
- [17] Sanat Ghosh, Vilas Patil, Amit Basu, Kuldeep, Achintya Dutta, Digambar A. Jangade, Ruta Kulkarni, A. Thamizhavel, Jacob F. Steiner, Felix von Oppen, and Mandar M. Deshmukh. High-temperature josephson diode. *Nature Materials*, 23:612–618, 5 2024. ISSN 1476-1122. doi:10.1038/s41563-024-01804-4.
- [18] Stefan Ilić, Pauli Virtanen, Daniel Crawford, Tero T. Heikkilä, and F. Sebastián Bergeret. Superconducting diode effect in diffusive superconductors and josephson junctions with rashba spin-orbit coupling. *Physical Review B*, 110:L140501, 10 2024. ISSN 2469-9950. doi:10.1103/PhysRevB.110.L140501.
- [19] Jin-Xin Hu, Shuai A. Chen, and K. T. Law. Geometric and conventional contributions of superconducting

- diode effect: Application to flat-band systems. *Physical Review B*, 111:174513, 5 2025. ISSN 2469-9950. doi:10.1103/PhysRevB.111.174513.
- [20] Debmalya Chakraborty and Annica M. Black-Schaffer. Perfect superconducting diode effect in altermagnets. *Physical Review Letters*, 135:026001, 7 2025. ISSN 0031-9007. doi:10.1103/cv8s-tk4c.
- [21] Josep Ingla-Aynés, Yasen Hou, Sarah Wang, En-De Chu, Oleg A. Mukhanov, Peng Wei, and Jagadeesh S. Moodera. Efficient superconducting diodes and rectifiers for quantum circuitry. *Nature Electronics*, 8:411–416, 5 2025. ISSN 2520-1131. doi:10.1038/s41928-025-01375-5.
- [22] Pavan Hosur. Digital logic from high-efficiency superconducting diodes, 2024. URL <https://arxiv.org/abs/2410.23352>.
- [23] Jiajun Ma, Ruiya Zhan, and Xiao Lin. Superconducting diode effects: Mechanisms, materials and applications. *Advanced Physics Research*, 4, 6 2025. ISSN 2751-1200. doi:10.1002/apxr.202400180.
- [24] Chao-Xing Liu. Unconventional superconductivity in bilayer transition metal dichalcogenides. *Physical Review Letters*, 118:087001, 2 2017. ISSN 0031-9007. doi:10.1103/PhysRevLett.118.087001.
- [25] Puhua Wan, Oleksandr Zheliuk, Noah FQ Yuan, Xiaoli Peng, Le Zhang, Minpeng Liang, Uli Zeitler, Steffen Wiedmann, Nigel E Hussey, Thomas TM Palstra, et al. Orbital fulde-ferrell-larkin-ovchinnikov state in an ising superconductor. *Nature*, pages 1–6, 2023.
- [26] Dong Zhao, Lukas Debbeler, Matthias Kühne, Sven Fecher, Nils Gross, and Jurgen Smet. Evidence of finite-momentum pairing in a centrosymmetric bilayer. *Nature Physics*, 19:1599–1604, 11 2023. ISSN 1745-2473. doi:10.1038/s41567-023-02202-4.
- [27] Uddalok Nag, Jonathan Schirmer, Enrico Rossi, Chao-Xing Liu, and J. K. Jain. Phase diagram of a bilayer superconductor under an in-plane magnetic field. *Physical Review B*, 112:144513, 10 2025. ISSN 2469-9950. doi:10.1103/gnth-5ssq.
- [28] J. M. Lu, O. Zheliuk, I. Leermakers, N. F. Q. Yuan, U. Zeitler, K. T. Law, and J. T. Ye. Evidence for two-dimensional ising superconductivity in gated mos 2. *Science*, 350:1353–1357, 12 2015. ISSN 0036-8075. doi:10.1126/science.aab2277.
- [29] Yu Saito, Yasuharu Nakamura, Mohammad Saeed Bahramy, Yoshimitsu Kohama, Jianting Ye, Yuichi Kasahara, Yuji Nakagawa, Masaru Onga, Masashi Tokunaga, Tsutomu Nojima, Youichi Yanase, and Yoshihiro Iwasa. Superconductivity protected by spin-valley locking in ion-gated mos2. *Nature Physics*, 12:144–149, 2 2016. ISSN 1745-2473. doi:10.1038/nphys3580.
- [30] Xiaoxiang Xi, Zefang Wang, Weiwei Zhao, Ju-Hyun Park, Kam Tuen Law, Helmuth Berger, László Forró, Jie Shan, and Kin Fai Mak. Ising pairing in superconducting nbse2 atomic layers. *Nature Physics*, 12:139–143, 2 2016. ISSN 1745-2473. doi:10.1038/nphys3538.
- [31] Sayak Bhowmik and Arijit Saha. Topological majorana zero modes and the superconducting diode effect driven by fulde-ferrell-larkin-ovchinnikov pairing in a helical shiba chain. *Physical Review B*, 111:L161402, 4 2025. ISSN 2469-9950. doi:10.1103/PhysRevB.111.L161402.
- [32] RP Kaur, DF Agterberg, and Manfred Sigrist. Helical vortex phase in the noncentrosymmetric CePt 3 Si. *Physical Review Letters*, 94(13):137002, 2005.
- [33] M Smidman, MB Salamon, HQ Yuan, and DF Agterberg. Superconductivity and spin-orbit coupling in non-centrosymmetric materials: a review. *Reports on Progress in Physics*, 80(3):036501, 2017.
- [34] K. V. Samokhin. Helical states and solitons in noncentrosymmetric superconductors. *Physical Review B*, 89:094503, 3 2014. ISSN 1098-0121. doi:10.1103/PhysRevB.89.094503.
- [35] See supplemental material, which provides further details and proofs supporting certain statements in the main text. Supplemental Material. URL will be inserted by publisher.
- [36] Milton Abramowitz and Irene A Stegun. *Handbook of mathematical functions: with formulas, graphs, and mathematical tables*, volume 55. Courier Corporation, 1965.
- [37] A.C. Scott, F.Y.F. Chu, and D.W. McLaughlin. The soliton: A new concept in applied science. *Proceedings of the IEEE*, 61(10):1443–1483, 1973. doi:10.1109/PROC.1973.9296.
- [38] Egon Sohn, Xiaoxiang Xi, Wen-Yu He, Shengwei Jiang, Zefang Wang, Kaifei Kang, Ju-Hyun Park, Helmuth Berger, László Forró, Kam Tuen Law, Jie Shan, and Kin Fai Mak. An unusual continuous paramagnetic-limited superconducting phase transition in 2d nbse 2. *Nature Materials*, 17:504–508, 6 2018. ISSN 1476-1122. doi:10.1038/s41563-018-0061-1.
- [39] Sergio C de la Barrera, Michael R Sinko, Devashish P Gopalan, Nikhil Sivadas, Kyle L Seyler, Kenji Watanabe, Takashi Taniguchi, Adam W Tsen, Xiaodong Xu, Di Xiao, et al. Tuning Ising superconductivity with layer and spin-orbit coupling in two-dimensional transition-metal dichalcogenides. *Nature Communications*, 9(1):1–8, 2018.

Supplemental Material for “Current Induced Switching of Superconducting Order and Enhancement of Superconducting Diode Efficiency”

Uddalok Nag,¹ Jonathan Schirmer,² Chao-Xing Liu,^{1,3} and J. K. Jain^{1,3}

¹*Department of Physics, 104 Davey Lab, The Pennsylvania State University, University Park, Pennsylvania 16802, USA*

²*Department of Physics, William & Mary, Williamsburg, Virginia 23187, USA*

³*Center for Theory of Emergent Quantum Matter, The Pennsylvania State University, University Park, Pennsylvania 16802, USA*

In this Supplementary Material, we provide the technical details and derivations supporting the results presented in the main text. In Sec. (S1), we derive the Ginzburg-Landau (GL) free energy from a microscopic bilayer negative- U Hubbard model using the Hubbard-Stratonovich transformation. The minimization of this free energy is discussed in Sec. (S2), where we map the problem onto the sine-Gordon equation and obtain solutions in terms of Jacobi elliptic functions. The subsequent sections explore specific limits of the theory: Sec. (S3) analyzes the low-magnetic-field regime to establish the linear dependence of the diode efficiency on the magnetic field ($\propto q_B$), while Sec. (S4) and Sec. (S5) examine the high-field limit to demonstrate how reciprocity is recovered as the layers effectively decouple. Finally, Sec. (S6) provides an analytical derivation of the interlayer vortex density in both the sparse and dense vortex limits, the former confirming the continuous nature of the BCS-FFLO transition.

S1: THE GINZBURG-LANDAU THEORY OF BILAYER SUPERCONDUCTOR

We start with a bilayer lattice model where each layer is described by a negative U Hubbard model

$$\mathcal{H}_l = -t \sum_{\langle i,j \rangle, \sigma} \hat{c}_{l,i,\sigma}^\dagger \hat{c}_{l,j,\sigma} - \mu \sum_{i,\sigma} \hat{c}_{l,i,\sigma}^\dagger \hat{c}_{l,i,\sigma} \quad (\text{S1})$$

$$- U \sum_i \hat{c}_{l,i,\uparrow}^\dagger \hat{c}_{l,i,\downarrow}^\dagger \hat{c}_{l,i,\downarrow} \hat{c}_{l,i,\uparrow},$$

with $U > 0$. The nearest neighbour interlayer coupling is given by

$$\mathcal{H}_\perp = -t_\perp \sum_{i,\sigma} (\hat{c}_{1,i,\sigma}^\dagger \hat{c}_{2,i,\sigma} + h.c.). \quad (\text{S2})$$

and the full Hamiltonian is given by

$$\mathcal{H} = \mathcal{H}_1 + \mathcal{H}_2 + \mathcal{H}_\perp.$$

The partition function is written as

$$\mathcal{Z} = \text{Tr}(e^{-\beta_T \mathcal{H}}), \quad (\text{S3})$$

where $\beta_T = 1/T$ and T is the temperature. We introduce Grassmannian fields c and c^* defined on each $\{l, i, \sigma\}$. The partition function can then be written as a path integral form

$$\mathcal{Z} = \int \mathcal{D}[c^*, c] e^{-S[c^*, c]} \quad (\text{S4})$$

with the action is given by

$$S = \int_0^{\beta_T} d\tau \left[\sum_{l,i,\sigma} c_{l,i,\sigma}^* (\partial_\tau - \mu) c_{l,i,\sigma} + \mathcal{H}[c^*, c] \right]. \quad (\text{S5})$$

Note that the Grassmannian fields are antiperiodic in imaginary time with the period β_T ,

$$c_{l,i,\sigma}(\beta_T) = -c_{l,i,\sigma}(0) \quad c_{l,i,\sigma}^*(\beta_T) = -c_{l,i,\sigma}^*(0).$$

For the quartic terms, we perform the Hubbard-Stratonovich transformation by introducing field $\Psi_{l,i}(\tau)$, which leads to

$$e^{U \int d\tau c_\uparrow^* c_\uparrow c_\downarrow c_\downarrow} = \int \mathcal{D}[\Psi, \Psi^*]$$

$$\exp \left[- \int d\tau \left(\frac{|\Psi|^2}{U} + \Psi c_\uparrow^* c_\downarrow^* + \Psi^* c_\downarrow c_\uparrow \right) \right]. \quad (\text{S6})$$

Thus, our partition function is expressed in terms of a path integral over both the Grassmannian fields and the new fields (Ψ) we introduced. Our strategy is to carry out the integration over the former to get an effective action in terms of the latter. We assume Ψ is uniform in space and imaginary time: $\Psi_{l,i}(\tau) \rightarrow \Psi_l$. We will later allow Ψ to vary slowly to compute the kinetic energy term of the GL free energy.

The action for each layer becomes

$$S_l' = \int_0^{\beta_T} d\tau \left[\sum_{l,i,\sigma} c_{l,i,\sigma}^* (\partial_\tau - \mu) c_{l,i,\sigma} - t \sum_{\langle i,j \rangle, \sigma} c_{l,i,\sigma}^* c_{l,j,\sigma} \right.$$

$$\left. + \sum_i \left(\frac{|\Psi_l|^2}{U} + \Psi_l c_{l,i,\uparrow}^* c_{l,i,\downarrow}^* + \Psi_l^* c_{l,i,\downarrow} c_{l,i,\uparrow} \right) \right]. \quad (\text{S7})$$

We also have the part of the action for interlayer tunnel-

ing

$$\begin{aligned} S'_\perp &= \int_0^{\beta T} d\tau \mathcal{H}_\perp[c^*, c] \\ &= \int_0^{\beta T} d\tau \left[-t_\perp \sum_{i,\sigma} \left(c_{1,i,\sigma}^* c_{2,i,\sigma} + c_{2,i,\sigma}^* c_{1,i,\sigma} \right) \right]. \end{aligned} \quad (\text{S8})$$

The full action is given by $S' = S'_1 + S'_2 + S'_\perp$

The new action is only bilinear in the Grassmannian fields, and hence, we can integrate them out from the partition function

$$\begin{aligned} \mathcal{Z} &= \int \mathcal{D}[c^*, c] e^{-S[c^*, c]} \\ &= \int \mathcal{D}[c^*, c] \mathcal{D}[\Psi^*, \Psi] e^{-S'[c^*, c, \Psi^*, \Psi]} \\ &= \int \mathcal{D}[\Psi^*, \Psi] e^{-S_{\text{eff}}[\Psi^*, \Psi]}. \end{aligned} \quad (\text{S9})$$

In the last line, we have integrated out the Grassman fields and introduced a new quantity

$$S_{\text{eff}}[\Psi^*, \Psi] := \beta T \sum_l \frac{|\Psi_l|^2}{U} - \sum_{\mathbf{k}, i\omega_n} \text{Tr} \ln G^{-1}(\mathbf{k}, i\omega_n, \Psi). \quad (\text{S10})$$

In the above equation, $\mathbf{k} = \frac{\pi}{L}(n_x, n_y)$, where $n_x, n_y = -(L-1), \dots, -1, 1, \dots, (L-1)$, and L is the size of the system in the x and y direction (L must be even). The fermionic Matsubara frequencies are given by: $\omega_n = \frac{(2m+1)\pi}{\beta}$, $m \in \mathbb{Z}$. The inverse Nambu Green's function can be written as, $G^{-1} = G_0^{-1} + (\Sigma(\Psi) + T)$, where,

$$G_0^{-1} = \begin{pmatrix} -i\omega_n + \xi_{\mathbf{k}} & 0 & 0 & 0 \\ 0 & -i\omega_n - \xi_{\mathbf{k}} & 0 & 0 \\ 0 & 0 & -i\omega_n + \xi_{\mathbf{k}} & 0 \\ 0 & 0 & 0 & -i\omega_n - \xi_{\mathbf{k}} \end{pmatrix} \quad (\text{S11})$$

$$\Sigma(\Psi) = \begin{pmatrix} 0 & \Psi_1 & 0 & 0 \\ \Psi_1^* & 0 & 0 & 0 \\ 0 & 0 & 0 & \Psi_2 \\ 0 & 0 & \Psi_2^* & 0 \end{pmatrix} \quad (\text{S12})$$

$$T = \begin{pmatrix} 0 & 0 & -t_\perp & 0 \\ 0 & 0 & 0 & t_\perp \\ -t_\perp & 0 & 0 & 0 \\ 0 & t_\perp & 0 & 0 \end{pmatrix}. \quad (\text{S13})$$

We treat Σ and T as perturbations, and expand:

$$\begin{aligned} \ln G^{-1} &= \ln G_0^{-1} + \ln(1 + G_0(\Sigma + T)) \\ &= \ln G_0^{-1} + \sum_{m=1}^{\infty} (-1)^{m+1} \frac{(G_0(\Sigma + T))^m}{m} \end{aligned} \quad (\text{S14})$$

The effective GL free energy $F[\Psi_1, \Psi_2] = \frac{S_{\text{eff}}}{\beta T}$:

$$\begin{aligned} F[\Psi_1, \Psi_2] &= \alpha(|\Psi_1|^2 + |\Psi_2|^2) + \beta(|\Psi_1|^4 + |\Psi_2|^4) \\ &\quad + J(\Psi_1 \Psi_2^* + \Psi_1^* \Psi_2) + \\ &\quad K(|\nabla \Psi_1|^2 + |\nabla \Psi_2|^2) \dots \end{aligned} \quad (\text{S15})$$

The coefficient α comes from the second order term in Eq. (S14), and β and J come from the fourth order term.

$$\alpha = \frac{1}{U} - \sum_{\mathbf{k}} \frac{1}{\xi_{\mathbf{k}}} \tanh\left(\frac{\beta T \xi_{\mathbf{k}}}{2}\right) \quad (\text{S16})$$

$$\beta = \sum_{\mathbf{k}} \frac{1}{8\xi_{\mathbf{k}}^3} \left[\tanh\left(\frac{\beta T \xi_{\mathbf{k}}}{2}\right) - \frac{1}{2} \beta T \xi_{\mathbf{k}} \text{sech}^2\left(\frac{\beta T \xi_{\mathbf{k}}}{2}\right) \right] \quad (\text{S17})$$

$$J = 2\beta t_\perp^2. \quad (\text{S18})$$

To get the gradient term in the GL free energy we must allow Ψ to slowly vary in space.

We can extract the temperature dependence of α from Eq. (S16),

$$\begin{aligned} \sum_{\mathbf{k}} \frac{1}{\xi_{\mathbf{k}}} \tanh\left(\frac{\beta T \xi_{\mathbf{k}}}{2}\right) &\approx N(0) \int_0^\Lambda d\xi \frac{1}{\xi} \tanh\left(\frac{\beta T \xi}{2}\right) \\ &= N(0) \int_0^{\frac{\beta T \Lambda}{2}} dx \frac{\tanh x}{x} \\ &= N(0) \ln(1.13\beta T \Lambda). \end{aligned} \quad (\text{S19})$$

Λ is just a cutoff and $N(0)$ is the density of states at the Fermi energy. We want $\alpha(T_c) = 0$. Therefore, $\frac{1}{U} = N(0) \ln(1.13\beta T_c \Lambda)$. Substituting, we get

$$\alpha = N(0) \ln\left(\frac{T}{T_c}\right) \approx \frac{N(0)}{T_c} (T - T_c). \quad (\text{S20})$$

After allowing Ψ to vary slowly and assuming that our dispersion relation is isotropic (which is true if we are close to the bottom of the band), we can also compute the coefficient K as

$$\begin{aligned} K &= 2 \sum_{\mathbf{k}} \left(v_{\mathbf{k}}^2 - \frac{1}{2} M_{\mathbf{k}} \xi_{\mathbf{k}} \right) \\ &\quad \times \frac{1}{8\xi_{\mathbf{k}}^3} \left[\tanh\left(\frac{\beta T \xi_{\mathbf{k}}}{2}\right) - \frac{1}{2} \beta T \xi_{\mathbf{k}} \text{sech}^2\left(\frac{\beta T \xi_{\mathbf{k}}}{2}\right) \right], \end{aligned} \quad (\text{S21})$$

where $v_{\mathbf{k}} := \nabla_{\mathbf{k}} \xi_{\mathbf{k}}$, and $M_{\mathbf{k}} := \nabla_{\mathbf{k}}^2 \xi_{\mathbf{k}}$. We tabulate one set of lattice parameters and the corresponding GL coefficients in Table S1.

TABLE S1: Microscopic lattice parameters and corresponding Ginzburg–Landau (GL) coefficients.

Lattice parameters					GL coefficients			
t	μ	U	t_{\perp}	δT	a	b	K	J
1.0	-0.02	3.2	0.227	0.01	-0.938	2.0306	0.09	0.209

S2: SINE GORDON EQUATION FOR INTERLAYER PHASE DIFFERENCE

The free energy in Eq. (2) of the main text can be split into two parts:

$$\Omega = \Omega_{\psi} + \Omega_{\theta}, \quad (\text{S22})$$

where,

$$\Omega_{\psi}(\psi_1, \psi_2) = \frac{1}{V_0} \int d^2\mathbf{r} \left[\sum_l \alpha_l \psi_l^2 + \frac{\beta}{2} \sum_l \psi_l^4 \right], \quad (\text{S23})$$

$$\Omega_{\theta}(\psi_1, \psi_2, q, \phi) = \frac{1}{V_0} \int d^2\mathbf{r} \left[\frac{\psi_1^2}{2m} \left(q - q_B + \frac{\nabla\phi}{2} \right)^2 + \frac{\psi_2^2}{2m} \left(q + q_B - \frac{\nabla\phi}{2} \right)^2 - 2J\psi_1\psi_2 \cos\phi \right]. \quad (\text{S24})$$

Ω_{ψ} only depends on amplitudes ψ_1 and ψ_2 , while Ω_{θ} controls the phase fluctuations. We can separate the action Ω_{θ} into

$$\Omega_{\theta} = \Omega_1 + \Omega_2 + \Omega_3, \quad (\text{S25})$$

where

$$\Omega_1 = \frac{1}{V_0} \int d^2\mathbf{r} \frac{1}{2m} (\psi_1^2 + \psi_2^2) q^2, \quad (\text{S26})$$

$$\Omega_2 = \frac{1}{V_0} \int d^2\mathbf{r} \left[\frac{1}{2m} (\psi_1^2 + \psi_2^2) \left(\frac{\nabla\phi}{2} - q_B \right)^2 - 2J\psi_1\psi_2 \cos\phi \right], \quad (\text{S27})$$

$$\Omega_3 = \frac{1}{V_0} \int d^2\mathbf{r} \frac{q}{m} (\psi_1^2 - \psi_2^2) \left(\frac{\nabla\phi}{2} - q_B \right). \quad (\text{S28})$$

Here Ω_1 only depends on q and is relevant to the calculation of supercurrent, Ω_2 describes the vortex dynamics of relative phase ϕ , and Ω_3 describes the coupling between the momentum q and the relative phase ϕ and can also contribute to supercurrent. Ω_3 is crucial for the coupling between the supercurrent and the interlayer vortices, which requires to break inversion symmetry between two layers since it includes the difference $\psi_1^2 - \psi_2^2$ between the SC order parameters in two layers.

We first consider Eq. (S27) at fixed ψ_1 and ψ_2 . After redefining $m' = 2m\psi_0^2/(\psi_1^2 + \psi_2^2)$ and $J' = \psi_1\psi_2J/\psi_0^2$, with $\psi_0 = (\psi_1 + \psi_2)/2$, we get the sine-Gordon type of action for Ω_2 ,

$$\Omega_2 = \frac{\psi_0^2}{L_x} \int dx \left[\frac{1}{m'} \left(\frac{1}{2} \partial_x \phi - q_B \right)^2 - 2J' \cos\phi \right] \quad (\text{S29})$$

Minimizing Ω_2 leads to,

$$\begin{aligned} \delta\Omega_2 &= \frac{1}{L_x} \int dx \left[\frac{1}{m'} \left(\frac{1}{2} \partial_x \phi - q_B \right) \partial_x (\delta\phi) + 2J' \sin\phi \delta\phi \right] \\ &= \frac{1}{L_x} \int dx \left[\frac{1}{2m'} (-\partial_x^2 \phi) + 2J' \sin\phi \right] \delta\phi. \end{aligned} \quad (\text{S30})$$

In the above steps, we used integral by parts, and dropped the boundary term. With $\delta\Omega_2 = 0$, we obtain the sine-Gordon equation:

$$-\frac{1}{2m'} \partial_x^2 \phi + 2J' \sin\phi = 0. \quad (\text{S31})$$

With the rescaling, $w = (4J'm')^{1/2}x$, Eq. (S31) becomes,

$$\partial_w^2 \phi = \sin\phi. \quad (\text{S32})$$

Equation (S32) can be rewritten as

$$\partial_w \left[\frac{1}{2} (\partial_w \phi)^2 + \cos\phi \right] = 0,$$

which gives,

$$\begin{aligned} \partial_w \phi(w) &= \pm \sqrt{C_0 - 2 \cos\phi} \\ \implies dw &= \pm \frac{d\phi}{\sqrt{C_0 - 2 \cos\phi}} \\ \implies \int_{w_0}^w dw &= \pm \int_{\phi(w_0)}^{\phi(w)} \frac{d\phi'}{\sqrt{C_0 - 2 \cos\phi'}}, \end{aligned}$$

where C_0 is a constant. By defining $\tilde{\phi} = \phi + \pi$, we have

$$\begin{aligned} w - w_0 &= \pm \int_{\tilde{\phi}(w_0)}^{\tilde{\phi}(w)} \frac{d\tilde{\phi}'}{\sqrt{C_0 + 2 \cos\tilde{\phi}'}} \\ &= \pm \frac{1}{\sqrt{C_0 + 2}} \int_{\tilde{\phi}(w_0)}^{\tilde{\phi}(w)} \frac{d\tilde{\phi}'}{\sqrt{1 - \frac{4}{C_0+2} \sin^2\left(\frac{\tilde{\phi}'}{2}\right)}} \end{aligned}$$

We choose the initial condition $\tilde{\phi}(w_0) = 0 \implies \phi(w_0) = -\pi$, and change integration variables to $\theta = \tilde{\phi}/2$, which gives

$$w - w_0 = \pm k \int_0^{\theta} \frac{d\theta'}{\sqrt{1 - k^2 \sin^2 \theta'}}, \quad (\text{S33})$$

where, $k = \frac{2}{\sqrt{C_0+2}}$. The right hand side of the above equation is the incomplete elliptic integral of the first kind, provided $k \in [0, 1]$, or $C_0 \geq 2$. The limiting cases of $k = 1$ or $C_0 = 2$ correspond to zero interlayer vortices.

As k decreases from 1 or C_0 increases from 2, the number of vortices in the system increases. The ground state is obtained by minimizing the total free energy (with all terms) with respect to k , ψ_1 , and ψ_2 .

The solution to Eq. (S33) is given by

$$\begin{aligned}\theta &= \text{am}\left(\pm \frac{1}{k}(w - w_0), k^2\right) \\ \phi(w) &= 2 \text{am}\left(\pm \frac{1}{k}(w - w_0), k^2\right) - \pi,\end{aligned}\quad (\text{S34})$$

where, $\text{am}(u, m)$ is the Jacobi-amplitude function [1, 2]. This gives the local minima of Ω_2 for a fixed ψ_1 and ψ_2 ,

$$\begin{aligned}\Omega'_2 &= \frac{\psi_0^2}{L_x} \int dx \left[\frac{1}{m'} \left(\frac{1}{2} \partial_x \phi - q_B \right)^2 - 2J' \cos \phi \right] \\ &= \frac{\psi_0^2}{m' L_x} \int dx \left[\left(\frac{1}{2} \partial_x \tilde{\phi} - q_B \right)^2 + 2J' m' \cos \tilde{\phi} \right]\end{aligned}$$

We can substitute Eq. (S34) in the expression for Ω_2 . Choosing $w_0 = 0$, and after some algebra, we get,

$$\begin{aligned}\Omega'_2 &= \frac{\psi_0^2}{m'} \left[q_B^2 - C_0 J' m' + \right. \\ &\quad \left. \frac{2}{L_x} \sqrt{J' m' (C_0 + 2)} \varepsilon(\sqrt{J' m' (C_0 + 2)} L_x, k^2) \right. \\ &\quad \left. \mp \frac{2q_B}{L_x} \text{am}(\sqrt{J' m' (C_0 + 2)} L_x, k^2) \right],\end{aligned}\quad (\text{S35})$$

where, $\varepsilon(u, m)$ is the Jacobi epsilon function [1, 2]. Choosing the negative sign in Eq. (S34) gives us the positive sign in the above equation and vice versa. For $q_B > 0$, choosing the positive sign in Eq. (S34) always gives us the lower energy solution and vice versa. For $q_B = 0$, it may seem there are two degenerate states corresponding to the two distinct solutions in Eq. (S34), but then the minimum occurs at $k = 1$, and the amplitude function is zero, giving us only one state. We have $\nabla \xi = 0$ in the FFLO state (in the gauge we have chosen in the main text). The free energy contribution from the overall phase is

$$\Omega_1 = \frac{1}{2m} (\psi_1^2 + \psi_2^2) q^2.\quad (\text{S36})$$

The coupling term Ω_3 between ξ and ϕ is given by,

$$\begin{aligned}\Omega_3 &= \frac{\psi_1^2 - \psi_2^2}{m} \frac{q}{L_x} \int dx \left(\frac{\partial_x \phi}{2} - q_B \right) \\ &= \frac{\psi_1^2 - \psi_2^2}{m} q \left(\frac{1}{L_x} \text{am}(\sqrt{J' m' (C_0 + 2)} L_x, k^2) - q_B \right).\end{aligned}\quad (\text{S37})$$

To consider the thermodynamic limit $L_x \rightarrow \infty$, we use the asymptotic behavior of $\varepsilon(u, m)$ and $\text{am}(u, m)$,

$$\lim_{L_x \rightarrow \infty} \frac{1}{L_x} \varepsilon(aL_x, k^2) = a \frac{E(k^2)}{K(k^2)}$$

$$\lim_{L_x \rightarrow \infty} \frac{1}{L_x} \text{am}(aL_x, k^2) = a \frac{\pi}{2K(k^2)},$$

where, $K(m)$ and $E(m)$ are the complete elliptic integrals of the first and second kind, respectively.

Using the above expressions and substituting the expressions for J' , m' , and C_0 we obtain,

$$\begin{aligned}\Omega_2 &= \frac{q_B^2}{2m} (\psi_1^2 + \psi_2^2) + A(k) \psi_1 \psi_2 \\ &\quad - B(k) q_B \left(\frac{\psi_1 \psi_2}{2} (\psi_1^2 + \psi_2^2) \right)^{1/2},\end{aligned}\quad (\text{S38})$$

$$\Omega_3 = \frac{\psi_1^2 - \psi_2^2}{2} q \left[B(k) \left(\frac{2\psi_1 \psi_2}{\psi_1^2 + \psi_2^2} \right)^{1/2} - \frac{2q_B}{m} \right],\quad (\text{S39})$$

where,

$$A(k) = 2J(1 - 2/k^2 + (4/k^2)(E(k^2)/K(k^2))),\quad (\text{S40})$$

$$B(k) = (2/k)(J/m)^{1/2}(\pi/K(k^2)).\quad (\text{S41})$$

The other terms remain unchanged.

For a fixed q we minimize the free energy with respect to k , ψ_1 , and ψ_2 , and obtain the ground state. When the minimum occurs at $k = 1$, there are no vortices in the system and we call this the BCS state. When the minimum occurs at $k < 1$, there are interlayer vortices, and the system is in the FFLO state. The current through the system is then determined from Eq. (5) in the main text.

S3: THE LOW MAGNETIC FIELD LIMIT

In this section we analyze the behaviour of η in the low q_B regime. We know from numerical calculations that in this regime the system prefers to be in the BCS state ($\nabla \phi = 0$). So in this section, we may restrict ourselves to the BCS saddle and rewrite the free energy as

$$\begin{aligned}\Omega_{\text{BCS}} &= \sum_{l=1,2} \left[\alpha_l \psi_l^2 + \frac{\beta}{2} \psi_l^4 + \frac{\psi_l^2}{2m} (q + (-1)^l q_B)^2 \right] \\ &\quad - 2J \psi_1 \psi_2.\end{aligned}\quad (\text{S42})$$

The current is given by,

$$I_x = \frac{2e}{m} [(\psi_1^2 + \psi_2^2)q - (\psi_1^2 - \psi_2^2)q_B].\quad (\text{S43})$$

We define the following quantities,

$$a_1(q, q_B) = \alpha_1 + \frac{(q - q_B)^2}{2m},\quad (\text{S44})$$

$$a_2(q, q_B) = \alpha_2 + \frac{(q + q_B)^2}{2m}.\quad (\text{S45})$$

Using these newly defined quantities, Eq. (S42) can be rewritten as

$$\Omega_{\text{BCS}} = a_1\psi_1^2 + \frac{\beta}{2}\psi_1^2 + a_2\psi_2^2 + \frac{\beta}{2}\psi_2^2 - 2J\psi_1\psi_2 \quad (\text{S46})$$

The BCS saddle is determined by minimizing the expression in Eq. (S46) with respect to ψ_1 and ψ_2 , which yields the following coupled equations,

$$a_1(q, q_B)\psi_1 + \beta\psi_1^3 - J\psi_2 = 0, \quad (\text{S47})$$

$$a_2(q, q_B)\psi_2 + \beta\psi_2^3 - J\psi_1 = 0. \quad (\text{S48})$$

In the main text, we defined the critical currents I_c^\pm at a fixed q_B as the magnitude of the maximum and minimum value of I_x as a function of q respectively. Let $q_\pm(q_B)$ be the values of q for which these extremum values are achieved. That is,

$$I_c^+(q_B) = I_x(q_+(q_B), q_B), \quad (\text{S49})$$

$$I_c^-(q_B) = I_x(q_-(q_B), q_B). \quad (\text{S50})$$

We wish to obtain a small q_B expansion for the critical currents. Let $q_+(0) = q_0$, and from symmetry of Ω_{BCS} , we know that $q_-(0) = -q_0$. Let $I_c^+(0) = I_0 = -I_c^-(0)$. Then, for small q_B ,

$$I_c^+(q_B) = I_0 + \partial_q I_x|_{(q_0,0)}\delta q_0 + \partial_{q_B} I_x|_{(q_0,0)}q_B + O(q_B^2). \quad (\text{S51})$$

But, by definition, $\partial_q I_x|_{(q_0,0)} = 0$. Therefore,

$$I_c^+(q_B) = I_0 + \partial_{q_B} I_x|_{(q_0,0)}q_B + O(q_B^2). \quad (\text{S52})$$

Similarly,

$$I_c^-(q_B) = I_0 - \partial_{q_B} I_x|_{(-q_0,0)}q_B + O(q_B^2). \quad (\text{S53})$$

Now, $\Omega_{\text{BCS}}(q, q_B) = \Omega_{\text{BCS}}(-q, -q_B)$. Since $I_x = 2e\partial_q \Omega_{\text{BCS}}$, $\partial_{q_B} I_x(q_0, 0) = \partial_{q_B} I_x(-q_0, 0)$. Let us call this quantity I'_0 . Using the formula for the diode efficiency from Eq. (1) in the main text, we get,

$$\eta(q_B) \approx q_B \frac{I'_0}{I_0} \propto q_B \quad (\text{S54})$$

To determine the exact slope, one needs to solve the system of Eqs. (S47) and (S48) for $q_B = 0$ and arbitrary values of q , and obtain the value of the currents. Since it is a coupled system of non linear equations, this is best done numerically. But we have shown that close to zero magnetic field, the leading contribution to η in linear in q_B .

S4: THE HIGH MAGNETIC FIELD LIMIT

In this section, we carry out the minimization with respect to k in the high magnetic field limit, and see what happens to the diode efficiency, η . We already derived the full free energy in the sine-Gordon saddle in the previous section, given by Eqns. (S23),(S26),(S38),(S39). Below, we define

$$S = \psi_1^2 + \psi_2^2, \quad (\text{S55})$$

$$D = \psi_1^2 - \psi_2^2, \quad (\text{S56})$$

$$P = \psi_1\psi_2. \quad (\text{S57})$$

Using these quantities, we rewrite the action as

$$\Omega_1 = \frac{q^2}{2m}S, \quad (\text{S58})$$

$$\Omega_2 = \frac{q_B^2}{2m}S + A(k)P - B(k)q_B \left(\frac{PS}{2}\right)^{1/2}, \quad (\text{S59})$$

$$\Omega_3 = \frac{D}{2}q \left(B(k) \left(\frac{2P}{S}\right)^{1/2} - \frac{2q_B}{m} \right), \quad (\text{S60})$$

where $A(k)$ and $B(k)$ has been defined in the previous section. We minimize the action with respect to k with fixed ψ_1 and ψ_2 . By defining quantities $u = (2P/S)^{1/2}$ and $\epsilon = (qD)/S$, $\partial\Omega/\partial k = 0$ gives

$$uA'(k) = (q_B - \epsilon)B'(k). \quad (\text{S61})$$

At high q_B , k should be small. So we use the small k asymptotic behavior of the elliptic integrals,

$$A(k) \approx 2J \left(\frac{2}{k^2} - 1 - \frac{k^2}{4} + O(k^4) \right) \quad (\text{S62})$$

$$B(k) = \left(\frac{J}{m}\right)^{1/2} \left(\frac{4}{k} - k - \frac{5k^3}{16} + O(k^5) \right) \quad (\text{S63})$$

Substituting these expressions in Eq.(S61), and keeping only leading powers of k , we find that the free energy Ω is stationary with respect to k when:

$$k^* = \frac{2\sqrt{Jm}}{q_B - \epsilon}u \quad (\text{S64})$$

Before we substitute this in Ω to get the effective free energy, let us first see how $\phi(x)$ looks like in this limit. We have obtained the expression for $\phi(x)$ in Eq. S34. At large q_B , $k^2 \approx 0$. So,

$$\begin{aligned} \phi^*(x) &\approx 2 \operatorname{am} \left(\frac{\sqrt{4Jm'}}{k^*}x, 0 \right) - \pi \\ &= 2(q_B - \epsilon) \left(\frac{Jm'}{Jm} \right)^{1/2} \frac{x}{u} - \pi \\ &= 2(q_B - \epsilon)x - \pi, \end{aligned} \quad (\text{S65})$$

where, we have defined $\phi(x)|_{k=k^*} = \phi^*(x)$. So, when $q_B \gg q$, $\phi^*(x) \approx 2q_B x - \pi$.

To understand how the diode efficiency (η) behaves in this limit, we substitute $k = k^*$ given by Eq. (S64) and expand in orders of $(1/q_B)$. After some algebra, the free energy is given by

$$\Omega_{\text{eff}}(\psi_1, \psi_2, q) = \Omega_\psi - \frac{J^2 m}{q_B^2} \frac{4\psi_1^2 \psi_2^2}{\psi_1^2 + \psi_2^2} + \frac{q^2}{2m} \left(\psi_1^2 + \psi_2^2 - \frac{(\psi_1^2 - \psi_2^2)^2}{\psi_1^2 + \psi_2^2} - \frac{4Jm}{q_B^2} \left(\frac{\psi_1^2 - \psi_2^2}{\psi_1^2 + \psi_2^2} \right)^2 \psi_1 \psi_2 \right) + O\left(\frac{1}{q_B^3}\right), \quad (\text{S66})$$

where, Ω_ψ is given by Eq. (S23). From Eq. (S66), we note that up to $O(1/q_B^2)$, no odd powers of q survive in Ω_{eff} . This means that at high q_B , $\Omega_{\text{eff}}(q) \approx \Omega_{\text{eff}}(-q)$. Since the current through the superconductor is given by $I = 2e\partial\Omega_{\text{eff}}/\partial q$, this implies that the currents are reciprocal in this limit, and $\eta \rightarrow 0$ as $q_B \rightarrow \infty$.

S5: EFFECTIVE DECOUPLING OF LAYERS IN THE HIGH B LIMIT

In this section, we wish to recast the free energy in terms of dimensionless quantities to show that the $q_B \rightarrow \infty$ limit is equivalent to the $J \rightarrow 0$ limit, where the two layers are decoupled. We consider the $q = 0$ case first. The angular part of free energy, Ω_θ is

$$\Omega_\theta(\psi_1, \psi_2, q, \phi) = \frac{1}{L_x} \int dx \left[\frac{\psi_1^2 + \psi_2^2}{2m} \left(\frac{\partial_x \phi}{2} - q_B \right)^2 - 2J\psi_1\psi_2 \cos \phi \right]. \quad (\text{S67})$$

With $w = (4J'm')^{1/2}x$, $m' = 2m\psi_0^2/(\psi_1^2 + \psi_2^2)$, $J' = \psi_1\psi_2 J/\psi_0^2$, and $\psi_0 = (\psi_1 + \psi_2)/2$, we have shown earlier that this reduces the Euler-Lagrange equation to the standard sine-Gordon form with no dimension-ful quantities, given by Eq. (S32). Ω_θ becomes

$$\begin{aligned} \Omega_\theta &= \frac{\psi_0^2}{L_x} \int dx \left[\frac{1}{m'} \left(\frac{\partial_x \phi}{2} - q_B \right)^2 - 2J' \cos \phi \right] \\ &= \Gamma \int dw [(\partial_w \phi - \delta)^2 - 2 \cos \phi], \end{aligned} \quad (\text{S68})$$

where

$$\Gamma = \frac{1}{2\sqrt{2}L_x} \left(\frac{J}{m} \psi_1 \psi_2 (\psi_1^2 + \psi_2^2) \right)^{1/2}. \quad (\text{S69})$$

The action in the integral is only controlled by the dimensionless quantity

$$\delta = \frac{q_B}{\sqrt{Jm}} \left(\frac{\psi_1^2 + \psi_2^2}{2\psi_1\psi_2} \right)^{1/2}. \quad (\text{S70})$$

For high values of δ , the system would tend to prefer a non zero $\partial_w \phi$ to reduce the magnitude of the first term in the integral, and for small values of δ , the system would prefer $\phi = 0$ to minimize the second term. So the competition between the BCS and the FFLO states is controlled entirely by the parameter $\delta \propto q_B/\sqrt{J}$. Therefore, $q_B \rightarrow \infty$ limit is equivalent to the $J \rightarrow 0$ limit, where the

two layers are effectively decoupled. In this limit, since the two layers behave independently, the diode efficiency, $\eta = 0$.

If we bring back the terms containing q ,

$$\begin{aligned} \Omega_\theta &= \frac{\psi_0^2}{L_x} \int dx \left[\frac{1}{m'} \left(\frac{\partial_x \phi}{2} - q_B \right)^2 - 2J' \cos \phi + \frac{q^2}{m'} \right. \\ &\quad \left. \frac{2q}{m'} \frac{\psi_1^2 - \psi_2^2}{\psi_1^2 + \psi_2^2} \left(\frac{\partial_x \phi}{2} - q_B \right) \right] \end{aligned} \quad (\text{S71})$$

Note that the third term is constant in ϕ and the fourth term is a total derivative, so they do not affect the Sine-Gordon action. After doing a similar rescaling, and defining a dimensionless quantity

$$\delta_q = \frac{q}{\sqrt{Jm}} \frac{\psi_1^2 - \psi_2^2}{(2\psi_1\psi_2(\psi_1^2 + \psi_2^2))^{1/2}}, \quad (\text{S72})$$

we get the free energy

$$\begin{aligned} \Omega_\theta &= \Gamma \int dw \left[(\partial_w \phi - \delta)^2 - 2 \cos \phi + \delta_q^2 \left(\frac{\psi_1^2 + \psi_2^2}{\psi_1^2 - \psi_2^2} \right)^2 \right. \\ &\quad \left. + 2\delta_q (\partial_w \phi - \delta) \right]. \end{aligned} \quad (\text{S73})$$

The final two terms do not contribute to the Sine-Gordon equation, as the third term is a constant in ϕ and the final terms is total derivative in ϕ .

S6: THE VORTEX DENSITY AND ITS ASYMPTOTIC LIMIT

In this section, we derive the vortex density of the bilayer system in two limiting regimes. We consider first the high magnetic-field limit, and then the regime close to the critical magnetic field at which vortices enter the system. A vortex in this system is defined as whenever the relative phase between the two layers changes by 2π . From the thermodynamic limit of the Jacobi amplitude function, the relative phase from Eq. S34 is given by:

$$\phi(x) = \frac{2\pi\sqrt{J'm'}}{kK(k^2)}x \quad (\text{S74})$$

Hence, from this, the linear density of vortices in the system is given by

$$\rho = \frac{\sqrt{J'm'}}{kK(k^2)}. \quad (\text{S75})$$

We have already shown, that at high magnetic fields, $\phi(x) = 2q_B x - \pi$ in Eq. (S65), which gives the asymptotic value of $\rho \rightarrow q_B/\pi$. We wish to determine how ρ approaches this limit. We have shown that to leading order in q_B , the value of k that minimizes the free energy is given by Eq. S64. To determine higher order corrections to k^* , we define:

$$F(k) = k^3(uA'(k) - (q_B - \epsilon)B'(k)) \quad (\text{S76})$$

From Eq. (S61), we see that the minimization condition $\partial\Omega/\partial k = 0$ is equivalent to $F(k) = 0$. Let us substitute $k = k^* + \delta k$ in this equation. Expanding around $k = k^*$ yields $F(k^*) + F'(k^*)\delta k = 0$, so $\delta k = -(F(k^*)/F'(k^*))$. Keeping only the lowest order correction, we find $\delta k = -k^{*3}/4$. Substituting δk in Eq. (S75), we find the asymptotic behaviour of the density of vortices at high magnetic fields,

$$\rho_{\text{high}} = \frac{q_B}{\pi} - \frac{u^4}{4\pi} \frac{(Jm)^2}{q_B^3}. \quad (\text{S77})$$

We next investigate the other limit when the magnetic field is only slightly higher than the critical field at which vortices start entering. Before we do that, we can compute $A'(k)$ and $B'(k)$ as follows from Eqns. (S40) and (S41),

$$A'(k) = -\frac{8J}{k^3(1-k^2)} \frac{E^2(k^2)}{K^2(k^2)} \quad (\text{S78})$$

$$B'(k) = -2\pi \sqrt{\frac{J}{m}} \frac{E(k^2)}{k^2(1-k^2)K^2(k^2)} \quad (\text{S79})$$

This simplifies the minimization condition in Eq. (S61) as

$$q_B - \epsilon = \frac{4u}{\pi} \sqrt{Jm} \frac{E(k^2)}{k} \quad (\text{S80})$$

To compute the asymptotic behavior in the sparse vortex limit, we choose $k = 1 - \delta$, with $\delta \ll 1$. It is useful to define the quantity $k' = \sqrt{1 - k^2} \approx \sqrt{2\delta}$. For simplicity,

we can also drop the ϵ . The asymptotic expansion for $E(k^2)$ in the $k \rightarrow 1^-$ limit is

$$E(k^2) = 1 + \frac{k'^2}{2} \left(\ln\left(\frac{4}{k'}\right) - \frac{1}{2} \right) + \dots \quad (\text{S81})$$

Substituting Eq. (S81) in Eq. (S80), and keeping only leading contributions, we get

$$q_B = \frac{4u}{\pi} \sqrt{Jm} \left(1 + \delta \ln\left(\frac{4}{\sqrt{2\delta}}\right) \right). \quad (\text{S82})$$

In the limit $\delta \rightarrow 0^+$, $q_B \rightarrow \frac{4u}{\pi} \sqrt{Jm}$, which is, therefore, the critical magnetic field $q_{B,c}$. Solving Eq. (S82) for δ , and using the fact δ is small, we get

$$\delta = \frac{r}{\ln\left(\frac{4}{r}\right)}, \quad (\text{S83})$$

where, we have used $r = (q_B/q_{B,c}) - 1$. Substituting $k = 1 - \delta$ in Eq. (S75), we get the low vortex density behavior

$$\rho_{\text{low}} = \frac{2u\sqrt{Jm}}{\ln\left(\frac{8}{\left(\frac{q_B}{q_{B,c}} - 1\right)}\right)}. \quad (\text{S84})$$

From Eq.(S84), one can see the vortex density ρ approaches zero as $q_B \rightarrow q_{B,c}^+$, so we would expect the BCS-FFLO transition is continuous in our system.

-
- [1] Milton Abramowitz and Irene A Stegun. *Handbook of mathematical functions: with formulas, graphs, and mathematical tables*, volume 55. Courier Corporation, 1965.
- [2] A.C. Scott, F.Y.F. Chu, and D.W. McLaughlin. The soliton: A new concept in applied science. *Proceedings of the IEEE*, 61(10):1443–1483, 1973. doi: 10.1109/PROC.1973.9296.